



HAL
open science

Optimizing the dispersion of nanoparticulate TiO₂-based UV filters in a non-polar medium used in sunscreen formulations – The roles of surfactants and particle coatings

Riccardo Catalano, Armand Masion, Fabio Ziarelli, Danielle Slomberg, Jerome Laisney, Jason Unrine, Andrea Campos, Jérôme Labille

► To cite this version:

Riccardo Catalano, Armand Masion, Fabio Ziarelli, Danielle Slomberg, Jerome Laisney, et al.. Optimizing the dispersion of nanoparticulate TiO₂-based UV filters in a non-polar medium used in sunscreen formulations – The roles of surfactants and particle coatings. *Colloids and Surfaces A: Physicochemical and Engineering Aspects*, 2020, 599, 10.1016/j.colsurfa.2020.124792 . hal-02864484

HAL Id: hal-02864484

<https://hal.science/hal-02864484>

Submitted on 15 Sep 2020

HAL is a multi-disciplinary open access archive for the deposit and dissemination of scientific research documents, whether they are published or not. The documents may come from teaching and research institutions in France or abroad, or from public or private research centers.

L'archive ouverte pluridisciplinaire **HAL**, est destinée au dépôt et à la diffusion de documents scientifiques de niveau recherche, publiés ou non, émanant des établissements d'enseignement et de recherche français ou étrangers, des laboratoires publics ou privés.



Distributed under a Creative Commons Attribution - NoDerivatives 4.0 International License



Optimizing the dispersion of nanoparticulate TiO₂-based UV filters in a non-polar medium used in sunscreen formulations – The roles of surfactants and particle coatings

Riccardo Catalano^a, Armand Masion^a, Fabio Ziarelli^b, Danielle Slomberg^a, Jérôme Laisney^c, Jason M. Unrine^c, Andrea Campos^d, Jérôme Labille^{a,*}

^a Aix Marseille Univ, CNRS, IRD, INRA, Coll France, CEREGE, Aix-en-Provence, France

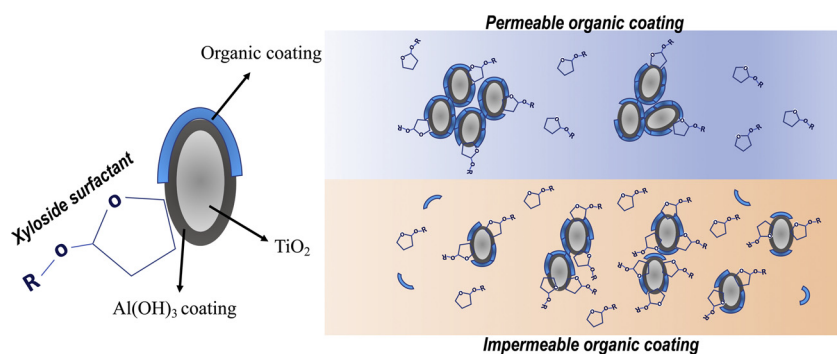
^b Aix-Marseille Univ, CNRS, Centrale Marseille, FSCM, 13397 Marseille, France

^c Univ Kentucky, Dept Plant & Soil Sci, 1100 S Limestone St, Lexington, KY 40546 USA

^d Aix Marseille Université, CNRS, Centrale Marseille, FSCM, CP2M, 13397 Marseille, France



GRAPHICAL ABSTRACT



ARTICLE INFO

Keywords:

Nanoparticle
Oil dispersion
Safe-by-design
Colloidal suspension
Octyldodecyl xyloside
NMR

ABSTRACT

Manufactured TiO₂ nanoparticles are widely used in cosmetics as UV blockers. The environmental risk associated with these Engineered Nanomaterials (ENMs) strongly depends on their concentration, aggregation state, and surface chemistry. Controlling these parameters in the sunscreen formulation is crucial in order to optimize the ENMs content and better understand their fate, transport, and toxicity at the product's end-of-life.

In the present work, the dispersion in sunscreen oil phase of four nanoparticulate UV filters having different coating characteristics was studied as a function of the oil composition. All the UV filters had a nano-TiO₂ core. Three of them were coated with a primary layer of aluminum (hydro)oxide and a secondary external layer of different polymers giving a hydrophobic character. The fourth UV-filter was coated with SiO₂ only, giving a hydrophilic character. The oil phase was composed of emollient oils and an emulsifying agent containing two surfactant molecules: Octyldodecyl xyloside (ODX) and PEG30 dipolyhydroxystearate (DHS). The ENMs were dispersed in the oil in the presence or absence of the emulsifying agent. Their aggregates size was evaluated, together with the speciation of the surface chemistry before and after the dispersion in oil.

We observed that the dispersion in oil of all the UV filters was enhanced by the emulsifying agent, as they were all more aggregated in the emollient oil free of emulsifier. The ODX surfactant played a major role in the ENM stabilization compared to the other oil phase components. The extent of interaction between nanoparticles

* Corresponding author.

E-mail address: labille@cerage.fr (J. Labille).

<https://doi.org/10.1016/j.colsurfa.2020.124792>

Received 27 November 2019; Received in revised form 26 March 2020; Accepted 27 March 2020

Available online 20 April 2020

0927-7757/ © 2020 The Author(s). Published by Elsevier B.V. This is an open access article under the CC BY-NC-ND license

(<http://creativecommons.org/licenses/by-nc-nd/4.0/>).

surface and ODX surfactant appeared to be mediated by the chemistry and the stability of both internal and external coatings of the ENM. The highest affinity was evidenced with the $\text{Al}(\text{OH})_3$ / dimethicone surface.

1. Introduction

Sunscreens provide effective protection against the damage caused by exposure to ultraviolet radiation (UVR) [1] which is dangerous for human skin, causing damages such as burns, aging, and even cancer [2]. These cosmetic products are highly consumed by the worldwide population as the sun care market constitutes 3% of the overall market of personal care products [3]. In order to absorb or reflect UVR, sunscreens contain UV filters, which can be organic (e.g., Avobenzone, Octocrylene) or mineral (TiO_2 , ZnO) and are dispersed in the formulation [4].

Contamination of the aquatic environment by UV filters is an increasing public concern due to the secondary effects of pharmaceuticals and personal care products potentially released in receiving aqueous systems, which may reach detectable and even toxic concentration levels [5,6]. Among these systems, contamination of the seawater environment is a crucial issue that needs to be studied [7], especially considering the increasing coral bleaching concerns in the recent years [8,9]. Between 6000 and 14,000 tons of sunscreen lotion are estimated to be released into coral reef areas each year bringing at least 10 % of the global reefs at risk of exposure, and approximately 40 % of coral reefs located along coastal areas at risk of exposure [10,9].

Mineral UV-filters are the only type of UV filter accepted in sunscreens labelled as BIO (or Natural) because they are considered safer for the consumer and the environment [11]. Moreover, the market of mineral-based sunscreens has largely shifted to nano-sized particles, not only because of their higher efficiency but also because of their transparency on the consumer's skin [12]. Nevertheless, their environmental impact still needs further investigation [11].

Some biological models have shown harmful effects in the presence of pure TiO_2 nanoparticles, at nearly field relevant concentrations [13,14]. The mineral filters used in sunscreens are usually coated with an internal mineral layer that prevents photocatalytic activity (e.g. Al_2O_3 ; SiO_2) and an external layer aimed at enhancing dispersion in the sunscreen formulation (e.g. PDMS; Stearic acid). Pure TiO_2 nanoparticles could thus be considered as analogues of the final aging stage of the mineral UV filters normally used in sunscreens. Indeed, it was shown that the external PDMS coating of certain mineral UV filters undergoes oxidation and desorption soon after contact with water, causing favored dispersion and thus higher bio-accessibility of the newly hydrophilic nanoparticles [15–17].

In this context of anthropic impact on the aquatic environment, a challenge remains in minimizing the risk associated with nanoparticulate mineral UV filters, i.e., decreasing their environmental hazard or exposition. While this could be achieved by modifying the chemistry of the filters or reducing their content in the formulation, altering the product efficacy to screen the UVR is not a feasible option. A compromise can be found by optimizing the nanoparticle dispersion in the formulation, since smaller primary particle sizes and finer particle dispersions were shown to result in a higher solar protection factor [18]. Controlling these parameters during the formulation is a crucial step in optimizing the efficiency of the nanoparticulate UV filters and it is certainly also an objective of cosmetic companies for economic reasons, because it allows a lower nanoparticle content with no decrease in the SPF. Following this approach, a lower environmental footprint can be obtained, and a safer-by-design product is developed. While the dispersion of nanoparticles in aqueous media has been well described by the theory of Deryagin, Landau, Verwey and Overbeek (DLVO), it is still challenging to model and optimize the dispersion of high-concentration nanoparticle suspensions in organic media [19]. Although

the coating selection is certainly one of the main strategies to achieve this, it was also observed that TiO_2 ENMs dispersion in organic media could be modulated by the adsorption of some specific molecules from the medium that would modify the ENMs interaction with the surrounding medium. This was evidenced for example with TiO_2 ENMs dispersion in a silicone oil, enhanced in the presence of agents bearing a perfluoroalkyl group [20].

Indeed, the interactions with the different sunscreen formulation ingredients can also influence the UV filter dispersion, as well as the stability of the entire product through particle-droplet interactions at the emulsion microstructure scale [21]. The actual extent of ENMs aggregation or dispersion strongly depends on the affinity of the filter surface, i.e. the external coating, for the dispersing medium or the surrounding components inside. Depending on the formulation composition and desired properties, sunscreen can be an oil in water (O/W) or water in oil (W/O) emulsion [22]. For the most common lipophilic UV filters, an optimal dispersion is normally obtained in the oil phase where the emollient assumes high chemical affinity for the ENM. Surfactants (emulsifying agents) are also present, aimed at stabilizing the oil-water interface [23].

Although it is well known that certain surfactants are able to stabilize TiO_2 particles in aqueous phase [24–26], a knowledge gap remains at the design stage of the sunscreen where the surface interactions between mineral particles and surfactants take place in an oil medium, and may determine the efficacy of the entire product. As it was already argued for other types of ENMs [27], such interactions may also modify the transport and reactivity of manufactured nanoparticles in the aqueous environment, and thus their exposure and hazard at the end of product life cycle.

Our work was aimed at studying the dispersion capacity of nano- TiO_2 based UV filters in a common bio-sourced sunscreen oil, in order to give insights on the role of the emulsifier at the initial stage of the sunscreen development and on how it may control the nanoparticle behavior. In order to avoid any interference coming from the interaction with the other sunscreen components, such as water, we decided to focus on the oil phase, as it represents the first dispersing medium in which nanoparticles are introduced during the formulation process. We studied four commercial UV filters characterized by different external coatings, and analyzed the surface interactions with the components of the dispersing medium, such as emollient and emulsifier. The dispersion state of the filters in the oil was evaluated using Dynamic Light Scattering (DLS). The chemical characterization of the nanoparticle surface, before and after interaction with the sunscreen oil phase, was performed through Solid State Nuclear Magnetic Resonance (^{13}C and ^{29}Si) and Transmission Electron Microscopy equipped with Energy Dispersive X-ray Spectroscopy (TEM EDS). A novel methodology to recover and dry the aged nanoparticles after dispersion in the oil phase is hereby proposed.

2. Material and methods

2.1. Commercial nano TiO_2 based UV filters

Four commercial TiO_2 -based sunscreen UV filters were selected here, based on contrasted surface coatings. They were provided by the manufacturers as a dry powder. Scanning Electron Microscopy in high resolution (HR-SEM) was performed to characterize the primary particle sizes. 3–4 mg of each dry powder were dispersed on a carbon adhesive tab and analysed using Zeiss Gemini500-Field emission SEM (see *Supplementary information*). Images were recorded at low voltage

(1–5 kV) to be able to obtain surface sensitive image at nanoscale resolution. In order to evaluate the primary particle size of the different filters, the longer side length of 50 particles in the images was measured using ImageJ software. The primary particle sizes obtained for each commercial UV filter are reported in Table 1, together with the respective trade name, abbreviation and chemical compositions provided by the manufacturers. All have a heterogenous but comparable primary particle size, between 50 and 65 nm in average. They consist of a TiO₂ nanoparticulate core, coated with dimethicone (T-dim), simethicone (T-sim), stearic acid (T-ste) or silica (T-S) as the external layer. An internal mineral layer made of aluminum (hydr)oxide was also found on the hydrophobic candidates T-dim, T-sim and T-ste, sandwiched between the TiO₂ surface and the grafted polymer.

2.2. Oil dispersing medium preparation

The components constituting the typical sunscreen oil phase used in this work are reported in Table 2. They were provided by the respective suppliers. They consist of two emollient oils: *Cetiol LC*[™] (Coco-Caprylate/Caprate) and *Tegosoft P*[™] (Isopropyl palmitate) [28], and one emulsifying agent: *Easynov*[™] [29]. Isopropyl palmitate is broadly used in cosmetics as a dispersing agent for both organic and mineral UV filters [30]. The emulsifying agent contains two types of surfactant: one polymeric, PEG30 dipolyhydroxystearate (DHS), and one glycoside non-ionic surfactant octyldodecyl xyloside (ODX). It is typically used to stabilize W/O cosmetic emulsions.

Tegosoft, Cetiol and Easynov were mixed together in a 2:2:1 ratio. The oil mixture (Phase A) was gently homogenized by magnetic stirring for 10 min. The nanoparticulate UV filter was then added to the oil phase in order to reach a concentration of 2.5 % w/w and was dispersed by mechanical agitation at ambient temperature for 10 min at 1000 rpm (which turned out to be the optimal speed in order to break particle aggregates; see *Supplementary Information*) using a *Heidolph Hei-Torque* 400 stirrer equipped with a pitcher blade impeller. For comparison, the same procedure was repeated in an oil phase free of emulsifier, in which the two emollient oils were mixed together with a 1:1 ratio (Phase B).

2.3. Elemental carbon analysis

In order to evaluate the % of carbon present in the three hydrophobic UV filters, a few milligrams (between 7–16) of the three pristine powders were placed in tin nacelles and analyzed using a Thermo-Fisher Scientific *FlashSmart*[™] elemental analyzer. A soil reference and aspartic acid, both provided by Thermo-Fisher, were used as calibration standards. The % of organic coating for each ENM was then calculated knowing the % of carbon and the molecular weight of the respective organic coating.

2.4. UV filter size distribution and UV absorbance in oil phase dispersions

Dynamic Light Scattering (DLS) intensity distributions of each UV filter suspension in oil were recorded right after the agitation step, in order to minimize any potential reaggregation before size measurement. A *Malvern Zetasizer Nano* (Malvern Instrument) was used. A 2 mL volume of the dispersion was analysed in a standard plastic disposable

cuvette. The measurements were performed in triplicates at 25 °C with 11 runs per measurement and 0.01 cumulant fit error tolerance. The viscosity used in the Stokes – Einstein relation, to calculate the hydrodynamic size of the UV filters dispersed in oil were measured as follows. Phases A and B were analysed through rheology measurement using an *Advanced Rheometer 1000* (TA Instrument) equipped with a 60 mm steel cone with 2° angle tip. The measurements were run in continuous speed rate from 0 to 100 s⁻¹ in 3 min. The measured viscosities were 7.45 ± 0.42 mPa for Phase A and 8.71 ± 0.24 mPa for Phase B,

The UV absorbance of each oil dispersion was also evaluated using the following methodology: ≅ 60 mg of the oily dispersion were deposited on a UV transmitting PMMA plate (50 × 50 cm; 5 μm medium roughness) and spread by light finger pressure all around the surface until a homogenous distribution was achieved. Absorbance spectra were then recorded in the UV range (270–400 nm) using a *Jasco v650* spectrophotometer equipped with an *ISV-922 60 mm diameter* Integrating Sphere. Each sample was analysed 4 times, rotating the PMMA plate a quarter turn between each replicate.

Single absorbance values at the fixed wavelength of 270 nm are presented in the results for each oily dispersion. Even-though these values do not equal the exact Solar Protection Factor (SPF), they give a rapid indication of the UV-screening efficacy of the nanoparticle-in-oil dispersion, since the SPF is proportional to the absorbance in the UV ray range [31].

2.5. Nanoparticle recovery after aging in the oil phase

Within dispersion in the oil, any component from the dispersing medium having high affinity for the UV filter surface may likely adsorb to it. In order to investigate such change in the ENM surface chemistry, an extraction protocol, adapted from Roweczyk et al. [32], was developed to recover and dry the nanoparticulate UV filters after aging in oil. The ENMs in oil dispersion was centrifuged at 11,200 g for 30 min (Jouan BR4i, Thermo). The pellet was separated from the oil supernatant and re-dispersed in 10 mL cyclohexane (Sigma Aldrich) in order to wash the oil components not strongly attached to the ENM surface. The ENMs were then centrifuged again for 30 min at 11,200 g. The pellets were separated from the supernatant and dried for 48 h using a Thermo Fisher freeze dryer. This drying procedure was required to have a particle powder enough withered to be suitable for a solid-state (ss) NMR analysis. Washing the ENMs with cyclohexane was essential, as the freeze-drying procedure alone was not able to remove the excess of oil phase from the pellets.

2.6. Chemical characterization of the oil and UV filters

Nuclear Magnetic Resonance (NMR) was used to characterize both the oil phases (¹³C NMR) and the nanoparticle coating before and after aging (¹³C and ²⁹Si NMR). For all the characterizations, ~100 mg of nanoparticle powder was placed in the rotor and analysed using a Bruker Advance III WB 400 solid state NMR spectrometer. In order to verify the chemical composition of the oil phases, ¹³C NMR spectra were recorded using low power decoupling sequence (Ipdec) with d1 = 10 s, number of scans (NS) = 2k, 3 kHz spin rate. ²⁹Si CPMAS

Table 1

Product name and chemical composition provided by the manufacturer for each of the four mineral UV filters together with their respective primary particle size measured by HR-SEM.

Product Name	Abbreviation	Manufacturer	Chemical composition	Primary particle size (nm)
T-Lite SF	T-dim	BASF	TiO ₂ (79–89%)/Al(OH) ₃ /Dimethicone	58.3 ± 10.8
Eusolex T-AVO	T-sil	Merck	TiO ₂ (79.6%)/SiO ₂	51.0 ± 10.6
Eusolex T-2000	T-sim	Merck	TiO ₂ (80.3%)/Al ₂ O ₃ /Simethicone	65.5 ± 12.8
Eusolex T-S	T-ste	Merck	TiO ₂ (73–79%)/Al ₂ O ₃ /Stearic Acid	64.4 ± 11.4

Table 2

Trade name and chemical composition provided by the manufacturer for each component of the oil phase.

Product name	Manufacturer	Function	Chemical composition
Tegosoft P	Evonik	Emollient oil	Isopropyl Palmitate
Cetiol LC	BASF	Emollient oil	Coco-Caprylate/Caprate
Easynov	SEPPIC	Emulsifying agent	Octyldodecanol; Octyldodecyl Xyloside; PEG-30 Dipolyhydroxystearate

were recorded at 79.5 MHz, 10 kHz spin rate. ^{13}C Cross-Polarization Magic Angle Spinning (CPMAS) spectra were recorded at 100.7 MHz, 10 kHz spin rate, 20k NS. Spectra simulations of oil phase components and particles organic coatings, together with peak integrations and gaussian fits of the experimental spectra, were performed using *Mest-Re NOVA* software (see *Supplementary Information*).

2.7. Elemental mapping and composition of the UV filters

The TiO_2 nanoparticles were examined by transmission electron microscopy (TEM) and scanning transmission electron microscopy (STEM) using a Talos F200X analytical electron microscope (Thermo Scientific, Waltham, MA, USA), operated at 200 keV and equipped with a four-element silicon drift detector (SDD)-based EDS system for quantitative chemical composition analysis and elemental distribution

mapping. Sample preparation was performed by dipping lacey carbon grids (Ted Pella, Redding, CA, USA) in 100 mg/L suspensions of nanoparticles previously sonicated for 15 min at maximum amplitude using a Misonix S-4000 cup-horn sonicator (Newton, CT, US) to ensure the optimal dispersion of the nanoparticulate powders.

3. Results and discussion

3.1. Emulsifying agent stabilizing UV filters dispersion

The size distributions of the nanoparticulate UV filters dispersed in Phase A are reported in Fig. 1 (solid lines). In all cases, they are relatively large and above the primary particle size, indicating polydisperse aggregation of the nanoparticles. The ENMs coated with stearic acid (a) or silica (b) are more aggregated than those coated with dimethicone

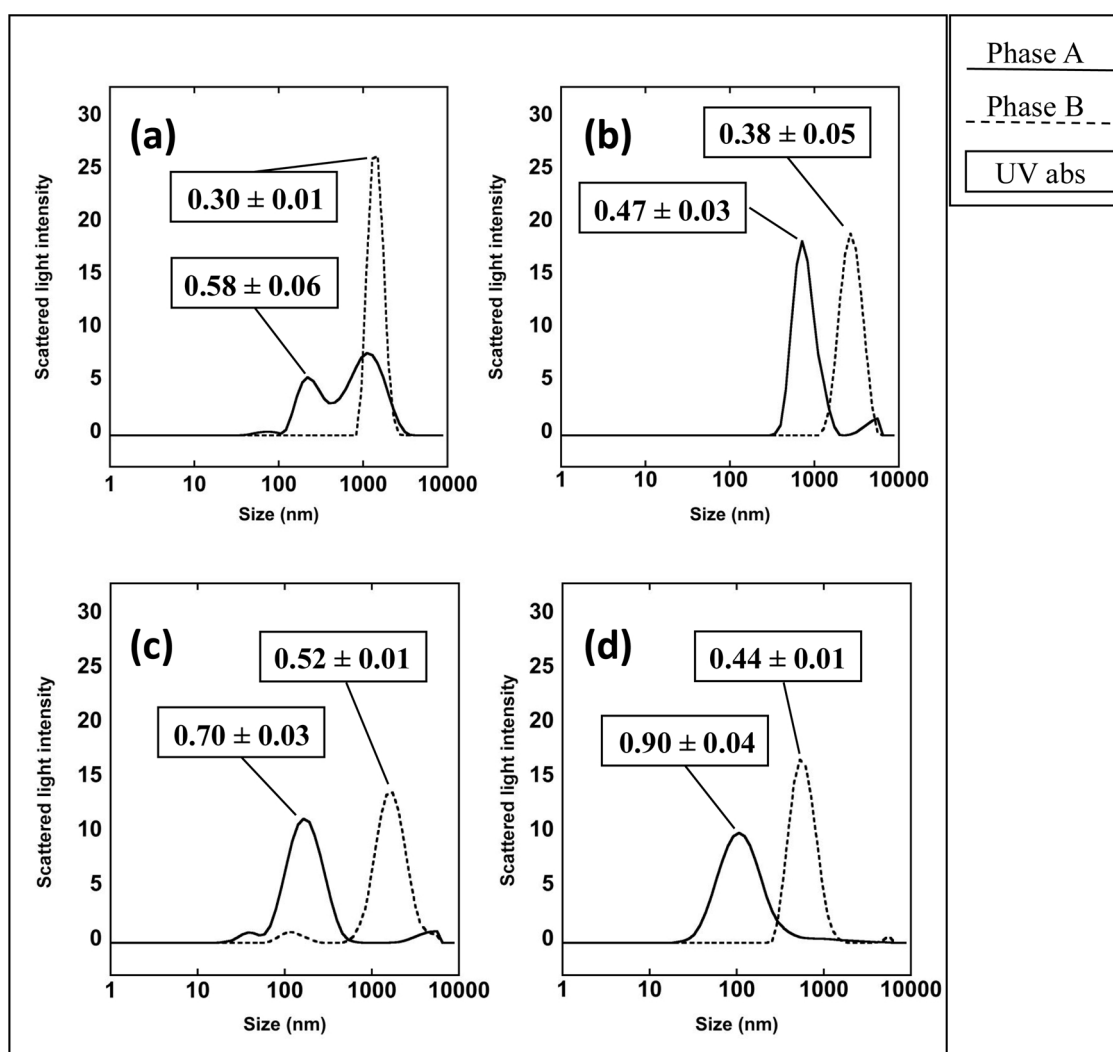


Fig. 1. Average hydrodynamic size distributions of the UV filters dispersed in Phase A (solid line) and Phase B (dashed line) for: (a) T-ste; (b) T-sil; (c) T-sim; (d) T-dim. Measurements were realised by DLS and are shown in intensity weight. The respective UV absorbances at 270 nm of the colloidal suspensions are reported inside the boxes for each distribution.

(c) or simethicone (d). The T-ste distribution appears bimodal at 220 and 1100 nm and the T-sil gives one peak at 800 nm, while the T-sim and T-dim distributions are centered on lower sizes around 100–200 nm. Significant aggregation was expected with the silica-coated nanoparticle, due to its hydrophilic surface, since in the oil dispersing medium there is no amphoteric surface charge driving any electrostatic inter-particle repulsion. However, the large aggregation of the T-ste UV filter is more surprising since the stearic acid coating is hydrophobic and was expected to have high affinity for the emollient components present in the oil (Isopropyl Palmitate; Coco-Caprylate).

The size distributions in the oil free of emulsifier (Phase B) (Fig. 1, dashed lines) clearly showed a general increase of the aggregate sizes for all the 4 UV filters compared to phase A. The narrower distributions in phase B suggest a more homogeneous aggregated state where the finer dispersed units around 100 nm have been totally incorporated into the larger ones of up to 1–2 μm in size. However, the aggregate sizes approached the nano-DLS detection limit, and the distribution widths are less trustworthy and thus impede an accurate signal interpretation.

Based on the Intensity mean values in the four DLS distributions, the shift of the aggregate size between Phase A and Phase B seems to depend on the UV filter type. The size shift is more pronounced in the case of T-sim (from 370 nm to 1719 nm) and T-dim (from 170 nm to 647 nm) while it is less evident for T-sil (from 1000 nm to 2700 nm) and T-ste (from 857 to 1437 nm). It is worthwhile noting that the presence of the emulsifier leads to a finer dispersion of the ENMs coated with simethicone or dimethicone (T-sim and T-dim) than for T-ste or T-sil, while without the emulsifier agent the four ENMs show similar aggregation states. The large aggregate size in phase B for all the four ENMs, suggests a relatively weak affinity of their respective surface coatings for the emollient oil used here. Yet, isopropyl palmitate is particularly recommended by the suppliers as a good dispersant oil phase for hydrophobically coated pigments in cosmetics preparations [28]. It should be noted that the agitation speed used to prepare the oil dispersion (1000 rpm) was high enough to break down the aggregates and bring most of the nanoparticles in contact with the solvent. As clearly shown by the UV absorbance (at 270 nm) values reported in Fig. 1, a loss of UV absorption is associated to the increasing ENMs aggregation state in all the Phase B formulations. The most important loss in UV absorbance with regard to values in Phase A, is measured for T-dim ENMs (- 45 % UV abs.), while for the other three filters the average loss is around 18 %. T-dim showed the best UV protection performances in Phase A formulation, likely because of their finest dispersion in this medium. These greater performances in Phase A could eventually explain the singular loss of screening efficacy of T-dim in Phase B medium compared with the other three UV filters. Nonetheless, the general trend of ENMs aggregation and UV absorbance of the formulations are in line with the previous findings of Tyner et al. [18]. Moreover, the large variability range in UV absorbance up to 45 %, confirms the need for optimal component coupling in the sunscreen formulation in the aim of minimizing the ENM aggregate size for maximizing the solar protection factor.

3.2. Characterization of the oil phases components

The oil phases A and B and the emulsifier used in this work were analysed using ^{13}C NMR spectroscopy, as shown in Fig. 2. The peak assignment was performed by comparing the experimental spectra with the predicted spectra of each component generated with *Mest-Re NOVA* software (see *Supplementary Information*).

The fingerprints of the two surfactants constituting the Easynov emulsifier are clearly seen in Fig. 2 (top). The signal at 100 ppm is attributed to the resonance of the anomeric carbon of the sugar moiety present in the ODX molecule. The small peak at 105 ppm is probably due to the resonance of the same anomeric carbon in a different conformation. The signal at 173 ppm is attributed to the resonance of the carboxylic carbon of the polymeric surfactant DHS. The other signals

between 75 and 60 ppm are due to the resonance of hydroxyl or ether groups present in both surfactant structures. The signal at 65 ppm is likely attributed to the hydroxyl group of the octyldodecanol, which is the solvent of the emulsifier agent. The ratio between the peak area of the anomeric carbon and the sum of the area of all the peaks of the emulsifying agent was used to determine the ratio of the ODX in the mixture. The same procedure was used to determine the ratio of the DPH, using the signal of its carboxylic carbon. This analysis revealed that the two surfactants and the octyldodecanol solvent, in the emulsifying agent, are in a ratio 1:1:8.

The ^{13}C NMR spectrum of the Phase B, containing only the two emollient oils, is reported in Fig. 2 (middle). The resonance of the carbonyl carbon is at 172.2 ppm for the caprate (Cetiol LC) and at 171.8 ppm for the isopropyl palmitate (Tegosoft). The peak at 67 ppm could be assigned to both the secondary C–OH group of the caprate and to the carbon next to the oxygen of the ester group isopropyl palmitate. The two signals at 64 ppm and 60 ppm are respectively assigned to the carbon next to the oxygen of the ester group and to the terminal C–OH group of the caprate oil. The spectrum of the Phase A, which is the mixture between the two emollient oils and the emulsifier, is reported in Fig. 2 (bottom). The region between 75 and 50 ppm is dominated by the two peaks at 67 and 64 ppm, which are likely associated to the isopropyl palmitate and caprate emollients. The other prominent signal at 70 ppm is assigned to octyldodecanol hydroxyl group (see *Supplementary Information*). The signals associated to the emulsifier are less intense and visible than in the top spectrum (Fig. 2 top), which is understandable as the Easynov constitutes 20 % w/w of the entire Phase A. Considering that each surfactant constitutes approximately 10 % of emulsifier, the concentration of each surfactant in the Phase A should be around 2% w/w. That is probably the reason why the ODX fingerprint at 100 ppm is barely visible in the Phase A spectrum.

3.3. Characterization of the pristine nanoparticulate UV filters

^{13}C NMR spectra of the pristine UV filters are shown in Fig. 3 a–d (bottom). For T-ste (Fig. 3 a), the presence of the stearic acid coating was confirmed by comparing the experimental spectra with the simulated Stearate spectra. The signal at 182 ppm is attributed to the carboxylic carbon resonance of the stearic acid molecule, together with the 6 peaks in the alkyl region associated to CH_2 and CH_3 groups of the stearate chain. The PDMS coating of T-sim and T-dim (Fig. 3 c,d) is

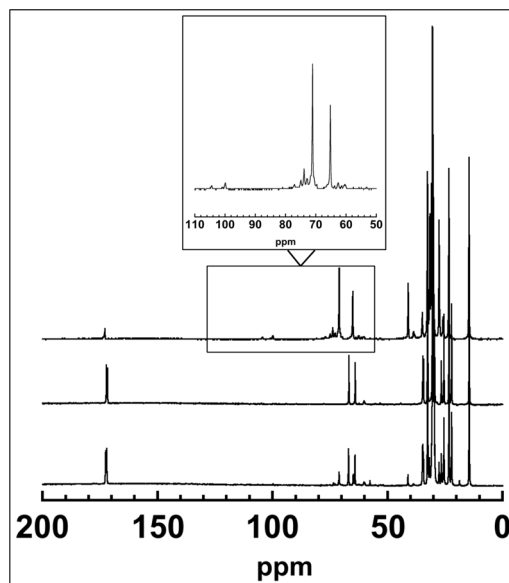


Fig. 2. ^{13}C NMR spectra of the Phase A oil (bottom); the Phase B oil free of emulsifier (middle); and the Easynov emulsifier (top).

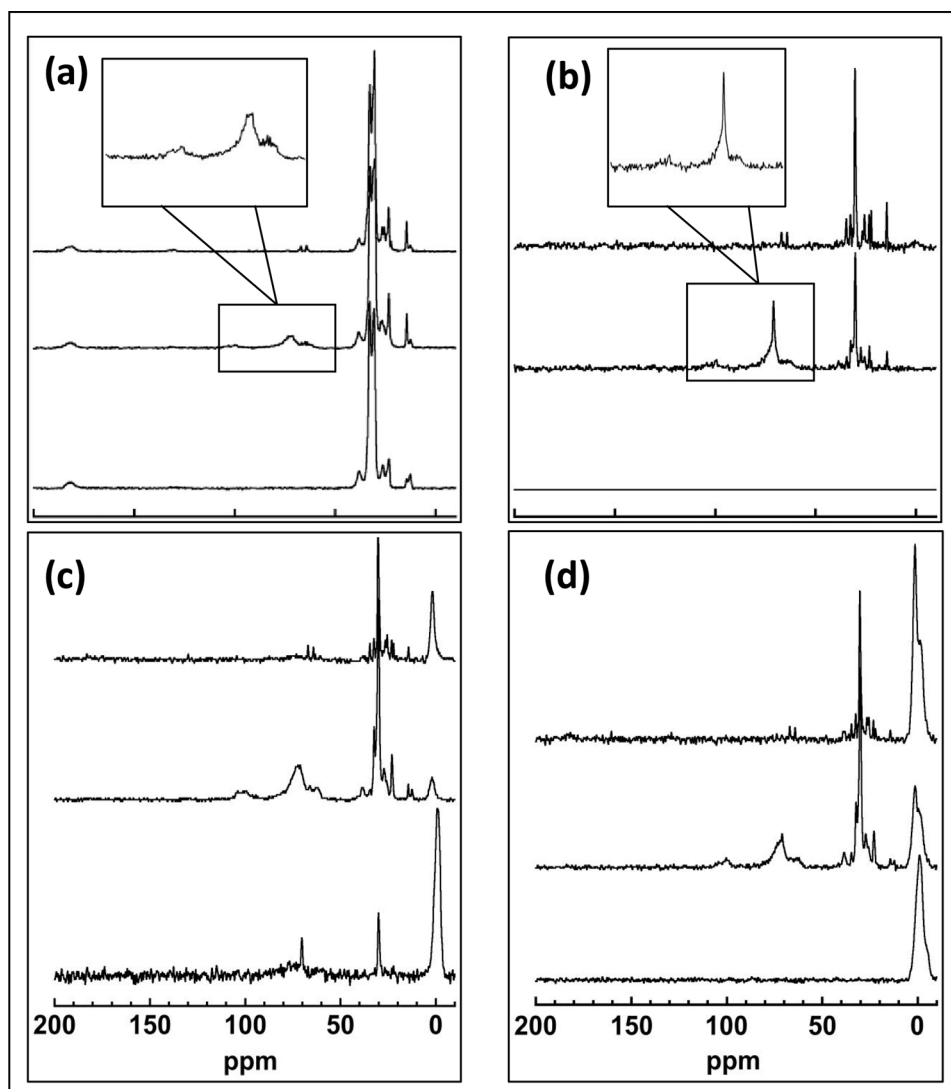


Fig. 3. ^{13}C NMR spectra for T-ste (a); T-sil (b); T-sim (c); and T-dim (d) UV filters; recorded on pristine ENMs (bottom), after aging treatment in Phase A (middle), or after aging treatment in Phase B (top).

confirmed by a clear signal at $-0,9$ ppm associated to the methyl groups bound to the SiO_2 units. In the T-sim spectra, the presence of two small signals at 70 and 30 ppm, could be due to propanol pollution. As expected, no carbon resonance signal was detected in the original T-sil spectra (Fig. 3 b), as they do not contain any organic coating.

^{29}Si NMR spectroscopy was performed on the UV filters containing silicon either in the form of silica or of PDMS (T-sil; T-dim; T-sim) and provided further characterization (Fig. 4). For T-dim filters (Fig. 4b), the resonance at 0 ppm corresponds to $\text{Si}(\text{CH}_3)_3$ terminal group and the resonance at -22 ppm is associated with $\text{SiO}(\text{CH}_3)_2$ main chain units of the PDMS polymer, while at -44 ppm the resonance signal is attributed to Si-O-Al linkages with the underlying $\text{Al}(\text{OH})_3$ coating. These results are in accordance with the findings of Auffan et al. on the same TiO_2 based UV filters [16]. For T-sil (Fig. 4c), the presence of the silica coating is confirmed by the resonance at -100 ppm associated to SiO_2 units. Surprisingly, the signal at -100 ppm of SiO_2 , which is a claimed component of commercial simethicone (PDMS + SiO_2), is missing in the spectrum of T-sim (Fig. 4a). Such absence of any SiO_2 signal was also confirmed using ATR-FTIR which provides a lower detection limit (data not shown). Furthermore, the signal at -44 ppm attributed to Si-O-Al linkages is missing, suggesting that the simethicone coating is not covalently bound to the ENM surface, but more likely weakly adsorbed.

3.4. The roles of emulsifier components and particle coatings

The ^{13}C NMR spectra for the four UV filters after aging in Phase A are reported in Fig. 3 (a,b,c,d) (middle). For each of the four ENMs, some signals related to organic molecules adsorbed to the ENM surface are clearly visible. These compounds were strongly attached to the nanoparticle surface considering that they remained bound through the treatment with cyclohexane followed by 48 h freeze drying. However, not all of the components of the phase A were visible in the spectra of the aged nanoparticles. Mainly the ODX molecule fingerprints was clearly distinguished, with the signal at 100 ppm of the anomeric carbon of the sugar moiety.

On the other hand, the missing signals in the carbonyl region of the NMR spectra, could exclude the presence of the other surfactant DPH as well as the two emollient oils. As all the oil phase components contain similar alkyl chains, with similar chain length and chemical structures, it is probable that the higher affinity for the nanoparticle surface of the ODX surfactant could come from its particular xyloside sugar moiety. In the aged T-sil spectrum, Fig. 3 (b – middle), the two narrow peaks at 70 and 30 ppm could also be associated to propanol contamination as in the pristine T-sim spectrum, Fig. 3 (c – bottom). This presumable contamination is covering part of the signals in the hydroxyl/ether region between 60 and 80 ppm and prohibited a quantitative analysis of the

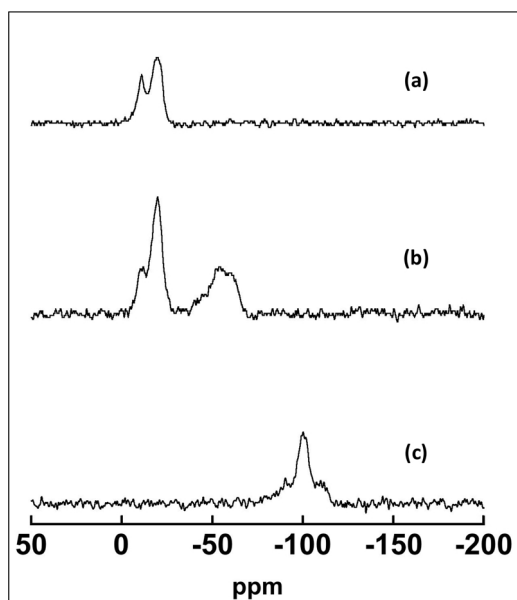


Fig. 4. ^{29}Si CPMAS NMR spectra of the pristine T-sim (a) ; T-dim (b); T-sil (c) UV filters.

spectra. This was however performed on the three other aged UV filters.

The peak integration in T-sim and T-dim aged spectra, Fig. 3 (c; d) (middle), enabled further understanding of the underlying mechanisms. The number of carbons associated to each peak was estimated based on the hypothesis that the signal at 100 ppm is only due to the resonance of the single anomeric carbon of the ODX sugar moiety attached to the ENM surface. This resulted in a number of carbons not related to the coating estimated at 20 in T-sim spectrum and 22 in T-dim spectrum. Even if we assume that all these carbons are only related to the surfactant molecule, this quantity is below the 25 carbons of the original ODX surfactant. We thus hypothesize that the surfactant molecule was partially degraded into smaller units.

It was not possible to clearly determine the mechanism that caused such degradation during the aging time or the extraction procedure. However, it is very unlikely that the addition of hexane during the washing procedure could have caused such type of reaction, as it is considered an inert solvent. It is instead more likely that the reaction could take place at the surface of the ENMs during the initial dispersion in oil. Further speculation about this hypothesis are handled afterwards.

In the spectrum of the T-ste UV filters aged in phase A, the stearic acid coating signal in the alkyl region partially covers the pattern of the organic molecules from phase A attached to the ENMs surface. It was thus impossible to determine the number of carbons associated to these compounds.

The ^{13}C NMR spectra for the ENMs aged in Phase B are shown in Figs. 3a–d (top). The two small peaks between 70–60 ppm are most likely due to the resonance of the alkyl carbons bound to the oxygen of the ester group of the two emollient oils: coco-caprylate and isopropyl palmitate. Even though, the signal associated to the resonance of the ester carbons itself was never present in all the four spectra. The reason could be that the quantity of emollients oils adsorbed on the ENMs surface was probably so low that ester signal could not be seen. Also, the similar shape and the intensity of these two peaks in all the 4 spectra suggest that the interaction does not change as function of the particle coating. This is in accordance with the size distribution of the ENMs in Phase B (Fig. 1) which showed similar aggregation state for the 4 types of nanoparticles and a larger size than in phase A. Nevertheless, the persistence of the emollient oil signals even after the recovery procedure, indicates that the interaction with the ENM surface is strong

enough to resist the recovery and drying procedure. This was not observed through aging in phase A, where only surfactant was added compared to phase B, but which resulted in a net ODX signal in the aged nanoparticles Fig. 3 (middle). This further supports the hypothesis that the prevalence of ODX signals in the spectra of the ENMs aged in Phase A, is due to a higher affinity of this surfactant for the ENM surface at the expense of the other component of the Phase A and not to a procedural artefact.

The resonance of the anomeric carbon of the octyldodecyl xyloside (100 ppm) was more pronounced in the T-sim and T-dim spectra, while it was less detected in the T-ste spectrum and barely visible in T-sil spectrum. In the spectra of the three hydrophobic UV filters aged in phase A, (Fig. 3 a, c, d middle), which did not contain any impurity signal, the area of each peak was determined using a gaussian fit. In each spectrum, the peak area of the anomer carbon was then divided by the total peak area in order to get the ratio of anomer signal and to compare its respective weight between the three candidates. The % of anomer signal ratio was 5.1 for T-sim, 3.8 for T-dim, and 3.2 and T-ste. The coating signal ratio, on the other hand, showed the opposite trend. The dimethicone signal ratio was 6.2 % in T-sim spectrum and 34 % in T-dim spectrum while the stearic acid ratio should be around 58 % in T-ste spectra, based on the signal ratio of the carboxylic carbon at 182 ppm. Thus, as the coating ratio decreases, the anomer ratio increases. This suggests that the interaction of the sugar moiety of the ODX may occur in the internal surface layer of the ENMs rather than over the organic outermost coating.

It is thus our hypothesis that the sugar moiety of the ODX interacts with the $\text{Al}(\text{OH})_3/\text{Al}_2\text{O}_3$ coating of the nanoparticles. Vilg -Ritter et al. already observed that aluminum polychlorosulfate PACS could selectively remove polysaccharide molecules from river waters [33]. Yang et al. and Chang et al. showed that Al^{3+} ions could strongly bind to the polysaccharide motifs of cell wall in pectin from Tobacco and Rice plants [34,35]. Efficient adsorption behavior of different monosaccharides onto Alumina surface were seen by Singh & Mohan [36,37] in aqueous solution. They reasoned that different types of interactions between the monosaccharides and the alumina surface could occur during the adsorption process, such as: electrostatic attraction (or repulsion) and hydrogen bonding. They also hypothesized that sucrose molecules can coordinate to Al atoms of “water coordinated” AlOH_2^+ groups by substitution of a water molecule, forming an organometallic complex.

How $\text{Al}(\text{OH})_3/\text{Al}_2\text{O}_3$ surfaces dispersed in oil here differ from the Al^{3+} ions and $\text{Al}(\text{OH})_3$ studied elsewhere in aqueous solution is not clear, as a knowledge gap remains on this latter systems. It is fair to say that electrostatic interactions (dipolar or ionic) would be more difficult, as an oil medium is less capable to allow acid-base equilibrium and ion stabilization. Hydrophobic bonding could also occur, but does not explain why the other components of the oil phase, which do contain hydrophobic tails, did not interact efficiently with the alumina surface. We thus hypothesize that complexation interaction between the aluminum oxide surface and the sugar moiety of ODX will be more probable in this oily system. Such type of bonding would also be more in accordance with the hypothesis of a partial breakdown of the surfactant molecule previously mentioned.

Moreover, considering the persistence of the signal at 100 ppm in Fig. 3 (middle), we assume that the rupture in the surfactant molecule should occur in the octyldodecyl chain. This would keep the O–C–O group intact, even if it is not certain whether the xyloside moiety was preserved or whether the pentose ring was successively opened generating an acetal group, which has similar chemical shift of anomer carbons.

Although proposing a mechanism for the surfactant break-down reaction was not the goal of this study, some hypothetical reactions are proposed here. The rupture of the molecule could be caused by a heterogeneous reaction at the $\text{Al}(\text{OH})_3/\text{Al}_2\text{O}_3$ surface. Organic reactions at the alumina surface are well established in literature and are very

useful in lab-scale synthesis because of their high selectivity and mild reaction conditions (ex: ambient temperature) [38]. While no specific studies on mono/di-saccharides degradation on aluminum oxides surfaces was already described, the formation of monosaccharides due to acetaldehyde polymerization (formose reaction) catalysed by Al_2O_3 was observed by Gabel & Ponnampuram in aqueous medium [39]. It is still unclear if alumina can also catalyse breakdown reactions of sugars, even if Reid & Orgel observed sugar degradation right after the formose reaction in similar conditions but using a carbonate-apatite catalyst [40].

Concerning the stabilization mechanism of the colloids in Phase A, we suppose that the ODX surfactant can act as charge control agent (CCA) on the ENM surface. CCAs increase the ionic conductivity of the system by creating free charges in solution or at particle surfaces. Surfactants are indeed capable of acting as charge control agents, affecting the interparticle interactions and the stability of the suspension in a non-polar system [41–43]. Yet, the mechanism leading to the particle charge stabilization is ambiguous [44]. In our system, particle aggregation being prevented by electrostatic repulsion should be the more realistic scenario considering the surfactant molecule breakdown at the Al_2O_3 surface, which would eventually reduce the alkyl tail length and minimize its hydrophobic stabilization within the oily medium or any steric hindrance between particles.

Due to the presence of propanol impurities in the aged T-sil ^{13}C NMR spectrum, it was not possible to perform a quantitative analysis that would define the potential break-down of the surfactant molecule on the silica surface. Nevertheless, such reaction was not expected here, since heterogeneous catalysis with pure SiO_2 has not been evidenced in the literature. Although the anomer carbon peaks in the spectrum of T-sil aged in phase A (100 ppm) appear feeble and less resolved, it is fair to say that the ODX molecule interacts with the silica surface, since a finer aggregation state of T-sil ENMs was measured in Phase A compared to Phase B (Fig. 1 b). Kwon et al. [45] studied the adsorption behavior of polysaccharide polymers (dextran) on silica and alumina surfaces. They observed that the mass of retained dextran was higher with alumina (83 ng/cm²) than with silica (9 ng/cm²), suggesting a higher affinity for the alumina. This agrees with our results showing ODX surfactant less detected on the T-sil surface than on T-dim or T-sim after aging in phase A.

The three UV filters T-dim, T-sim and T-ste all have an aluminum oxide coating which could likely favor such interaction with the sugar moiety of the ODX surfactant. Nevertheless, they displayed contrasted fates. This could be related to the stability of the respective polymer coatings. As previously mentioned, aged T-sil filters showed the lower coating signal ratio (6.2 %) compared to aged T-dim (34 %) and T-ste (58 %). This can be associated to a loss of the simethicone coating from the ENM surface during the dispersion stage. Indeed, the simethicone coating was not strongly bound to the particle surface, as seen from ^{29}Si NMR results (Fig. 4a) where no covalent linkage between the simethicone coating and the underlying alumina coating was detected, leading most likely to a lower stability of this external coating that could be partially removed during the dispersion procedure. Of note, even if a potential involvement of the cyclohexane washing procedure in the coating removal could not be excluded here (further investigation are needed to clarify this aspect), such effect would take place after the ENM aging in oil, and the preferential surface interaction with the ODX observed here would not be affected. The same process may take place in a lower extent with the T-dim ENMs, for which part of the dimethicone coating was covalently bound to the $\text{Al}(\text{OH})_3$ layer (Fig. 4b) constituting a more stable external layer. The stearic acid coating of T-ste probably constituted a denser and more stable surface layer, corroborated by its higher organic coating/ TiO_2 ratio (Table 3). This may prevent the surfactant molecules from diffusing and reaching the underlying $\text{Al}(\text{OH})_3$ surface. Higher steric hindrance may likely occur in the case of T-ste ENMs, because of the longer and bulkier C_{18} chains of the stearic acid coating in comparison with dimethicone single methyl

groups, although we do not have any information about the orientation of the different external coatings on the ENMs surface. In turn, the T-ste ENMs dispersion was less affected by the presence of the emulsifier agent (Fig. 1) and the pattern of this latter was less detected in the ^{13}C NMR spectra after aging in Phase A.

HR-TEM images of pristine and aged ENMs are presented in Fig. 5 (a;b;c;d). No significant differences in the size and shape are observed between the samples. T-sim ENMs aged in oil phase (Fig. 5 d), however, show a peculiar layer surrounding the particle surface that is not detected in the T-dim sample aged in Phase A. We do not have enough data to tell the nature and the origin of this layer even-though its thickness, and the fact that it is present just in the aged samples suggests that it could be an oil phase residue remaining attached to the particle surface. EDX characterization map of titanium, oxygen and aluminum on T-dim and T-sim ENMs before and after aging are presented in Fig. 5 (a1; b1; c1; d1). The mass ratio of aluminum in the sample areas analysed is reported in the red framed boxes. For both T-dim and T-sim ENMs, it remained unvaried before and after aging in Phase A (Fig. 5a1-b1 and Fig. 5c1-d1), suggesting that the aluminum oxide was not degraded during the whole aging and recovery processes. These results corroborate our previous hypothesis on the preferential interaction of the sugar moiety of the ODX surfactant with the aluminum oxide coating of the ENMs, which eventually constitutes a stable surface of interaction.

A sketched dispersion mechanism in Phase A medium is proposed in Fig. 6 for the four TiO_2 UV filters studied, based on these assumptions. Simethicone and Dimethicone coated ENMs (Fig. 6 (red)) showed the finer dispersion capacity. During the dispersion in oil, they could lose part of their coating, leaving a higher aluminum oxide surface available to interact with the ODX sugar moieties, which leads to a higher ENM dispersion stability. On another hand, the stearic acid coating on the T-ste ENMs (Fig. 5 (blue)) is more stable and remains mostly intact at the ENMs surface during the dispersion in oil. This leads to a lower extent of ODX surfactants reaching the alumina surface, and to a weaker particle dispersion stability in Phase A, i.e. larger aggregation. In T-sil ENMs (Fig. 6 (green)) there is no aluminum oxide but a SiO_2 coating. In absence of a secondary organic coating in the pristine material, this surface is fully accessible to the ODX molecules, nevertheless a weaker affinity takes place with silica compared to the aluminum oxide surface, resulting in a limited amount of adsorbed ODX and in a low dispersion stability, i.e. large aggregation.

4. Conclusions

The emulsifying agent Easynov™ favored the dispersion of four different commercial nanoparticulate UV filters in a realistic sunscreen oil phase. The extent of dispersion was shown to be influenced by the surface coating properties of the nanoparticles. Specific interaction between the octyldodecyl xyloside molecule and the four UV filters among the other oil phase components were observed, suggesting a key role of this surfactant in the stabilization of the colloidal system. This stabilization happened to be more efficient with mineral UV filters containing simethicone/dimethicone external coatings. After aging in the oil of the hydrophobic coated nanoparticles, an inverse relation was observed between the amount of external coating remaining at the ENMs surface and that of xyloside adsorbed. Thus, a specific interaction

Table 3
% of carbon and % of organic coating in the three UV filters T-dim, Tsim and T-ste.

Product name	% of carbon	% of organic coating
T-dim	1.11	3.42
T-sim	1.08	6.35
T-ste	7.38	9.21

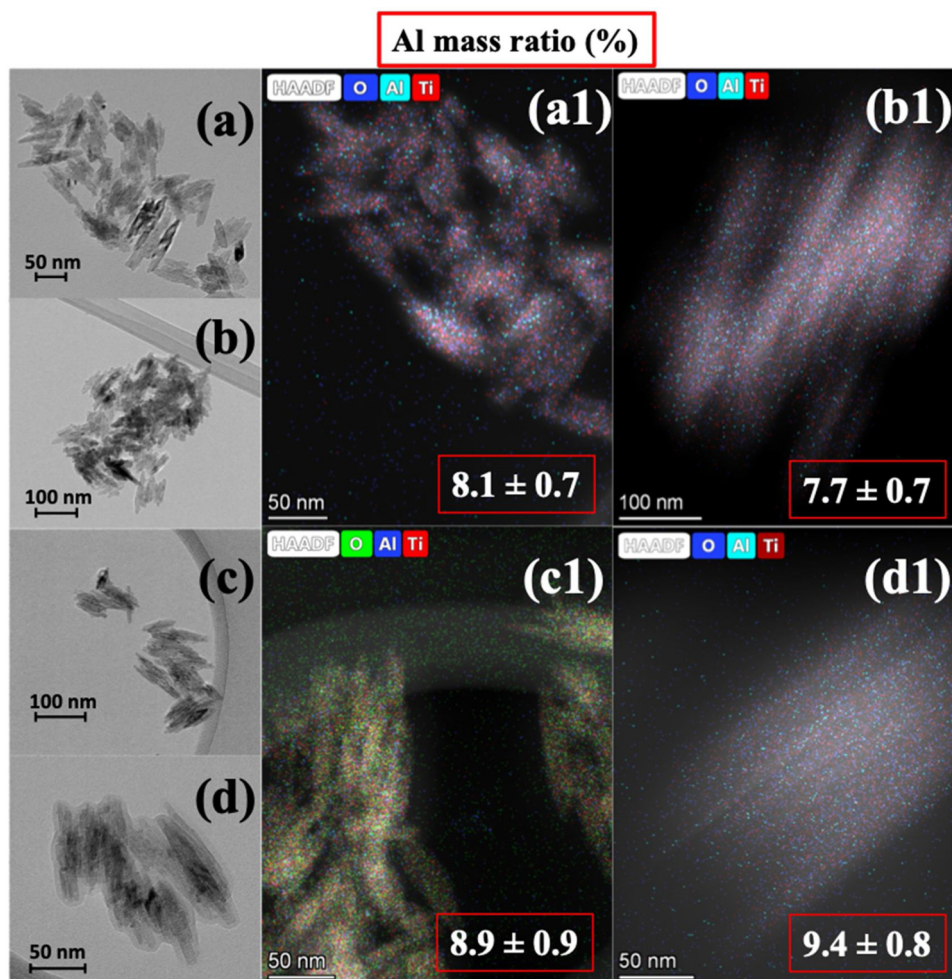


Fig. 5. HR TEM images of T-dim and T-sim pristine powders before (a; b) and after aging in Phase A (c; d). The respective EDX maps of oxygen; aluminum and titanium elements are reported in the images with a “1” label. The mass ratio (%) of aluminum in each area analysed is reported in the red framed boxes. (For interpretation of the references to colour in this figure legend, the reader is referred to the web version of this article).

with the internal $\text{Al}_2\text{O}_3/\text{Al}(\text{OH})_3$ coating was proposed.

In this work, surfactants normally used to stabilize W/O emulsions were highlighted to be also fundamental in stabilizing the nanoparticulate UV filters dispersions. A compromise needs to be considered between the stability of the mineral UV filter’s external coating and its capability to let the surfactant molecules diffuse into the inner spheres of the nanoparticle. In this light, T-dim ENMs showed the best

performance, given that the external PDMS coating was stable and not significantly degraded during the dispersion procedure but permeable enough to allow the diffusion of the ODX surfactant through the surface, leading to a finer ENMs dispersion and to an enhancement of the UV absorbance almost by a factor 2. This work brings light on the necessary step to optimize the use of nanomaterials in sunscreen product. Decreasing the amount of nanoparticulate UV filters in a sunscreen

Coating

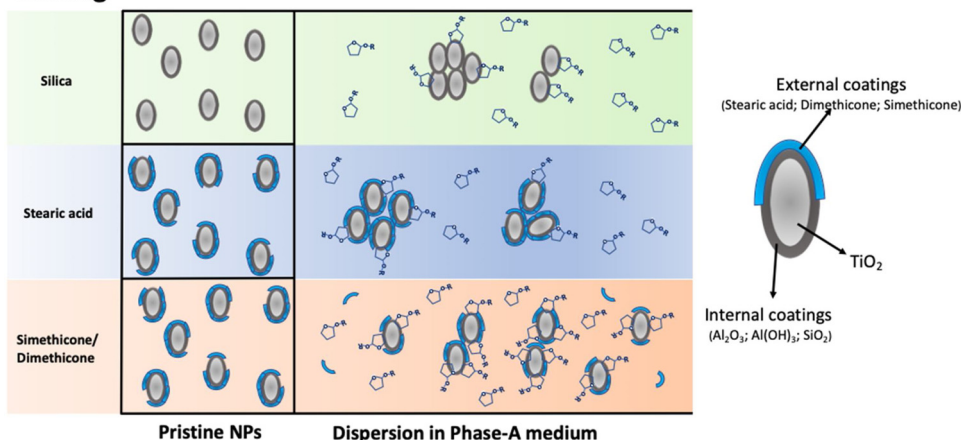


Fig. 6. Schematic representation of the different dispersion behaviors for the four tested UV filters: T-sim and T-dim (red); T-ste (blue); T-sil (green). The external coating is represented with blue blocs while the alumina or silica coating are the dark grey ovals. Differences on the quantity of blue pales between PDMS and stearic acid coated pristine ENMs, are used to emphasize the different capability of the two types of coating in shielding the inner spheres on the nanoparticle. (For interpretation of the references to colour in this figure legend, the reader is referred to the web version of this article).

formulation and better predicting their environmental fate and toxicity are key levers in the approach of minimizing the associated risk.

CRedit authorship contribution statement

Riccardo Catalano: Conceptualization, Data curation, Formal analysis, Investigation, Writing - original draft, Writing - review & editing. **Armand Masion:** Conceptualization, Data curation, Validation, Writing - original draft, Writing - review & editing. **Fabio Ziarelli:** Data curation, Formal analysis, Resources, Software. **Danielle Slomberg:** Conceptualization, Writing - original draft. **Jérôme Laisney:** Formal analysis. **Jason M. Unrine:** Resources, Software. **Andrea Campos:** Formal analysis, Resources, Software. **Jérôme Labille:** Conceptualization, Funding acquisition, Project administration, Resources, Supervision, Validation, Writing - original draft, Writing - review & editing.

Declaration of Competing Interest

The authors declare that they have no known competing financial interests or personal relationships that could have appeared to influence the work reported in this paper.

Acknowledgments

This work has received funding from the European Union's Horizon 2020 research and innovation programme under the Marie Skłodowska-Curie grant agreement No713750. It has also received funding from Excellence Initiative of Aix-Marseille University - A*MIDEX, a French "Investissements d'Avenir" program, through its associated Labex SERENADE project. This work is also a contribution to the OSU-Institut Pythéas and IPR Innove. The authors also acknowledge the CNRS for the funding of the PICS n°08322 SODA Light. The authors also want to thank: Nithavong Cam, Caroline Orneto and Helioscience in the person of Jean-Claude Hubaud for their precious contribution to this work.

Appendix A. Supplementary data

Supplementary material related to this article can be found, in the online version, at doi:<https://doi.org/10.1016/j.colsurfa.2020.124792>.

References

- [1] B.L. Diffey, Sunscreens and melanoma: the future looks bright, *Br. J. Dermatol.* 153 (2) (2005) 378–381, <https://doi.org/10.1111/j.1365-2133.2005.06729.x>.
- [2] A. Kricger, B.K. Armstrong, D.R. English, Sun exposure and non-melanocytic skin cancer, *Cancer Causes Control* 5 (4) (1994) 367–392, <https://doi.org/10.1007/BF01804988>.
- [3] U. Osterwalder, M. Sohn, B. Herzog, Global state of sunscreens: global state of sunscreens, *Photodermatol. Photoimmunol. Photomed.* 30 (2–3) (2014) 62–80, <https://doi.org/10.1111/phpp.12112>.
- [4] T.X. Hoang, I. Popa, Innovation in Inorganic UV Filters in Sunscreen, (2014).
- [5] P. Gago-Ferrero, M.B. Alonso, C.P. Bertozzi, J. Marigo, L. Barbosa, M. Cremer, E.R. Secchi, A. Azevedo, J. Lailson-Brito Jr., J.P.M. Torres, O. Malm, E. Eljarrat, M.S. Diaz-Cruz, D. Barceló, First Determination of UV Filters in Marine Mammals. Octocrylene Levels in Franciscana Dolphins, *Environ. Sci. Technol.* 47 (11) (2013) 5619–5625, <https://doi.org/10.1021/es400675y>.
- [6] H. Sharifan, D. Klein, A.N. Morse, UV Filters Interaction in the Chlorinated Swimming Pool, a New Challenge for Urbanization, a Need for Community Scale Investigations, *Environ. Res.* 148 (2016) 273–276, <https://doi.org/10.1016/j.envres.2016.04.002>.
- [7] J. Labille, D. Slomberg, R. Catalano, S. Robert, M.-L. Apers-Tremelo, J.-L. Boudenne, T. Manasfi, O. Radakovitch, Assessing UV filter inputs into beach waters during recreational activity: a field study of three french mediterranean beaches from consumer survey to water analysis, *Sci. Total Environ.* 706 (2020) 136010, <https://doi.org/10.1016/j.scitotenv.2019.136010>.
- [8] S.F. Heron, J.A. Maynard, R. van Hooindonk, C.M. Eakin, Warming trends and bleaching stress of the world's coral reefs 1985–2012, *Sci. Rep.* 6 (1) (2016) 38402, <https://doi.org/10.1038/srep38402>.
- [9] R. Danovaro, L. Bongiorno, C. Corinaldesi, D. Giovannelli, E. Damiani, P. Astolfi, L. Greci, A. Pusceddu, Sunscreens cause coral bleaching by promoting viral infections, *Environ. Health Perspect.* 116 (4) (2008) 441–447, <https://doi.org/10.1289/ehp.10966>.
- [10] C. Wilkinson, Status of Coral Reefs of the World, *Global Coral Reef Monitoring Network and Reef and Rainforest Research Centre*, Townsville, 2008.
- [11] D.M.E. Slijkerman, M. Keur, Sunscreen Ecoproducts: Product Claims, Potential Effects and Environmental Risks of Applied UV Filters, Wageningen Marine Research report C056/18, 2018, <https://doi.org/10.18174/457209>.
- [12] D.M. Berube, Rhetorical gamesmanship in the nano debates over sunscreens and nanoparticles, *J. Nanopart. Res.* 10 (S1) (2008) 23–37, <https://doi.org/10.1007/s11051-008-9362-7>.
- [13] G. Paterson, J.M. Ataria, M.E. Hoque, D.C. Burns, C.D. Metcalfe, The toxicity of titanium dioxide nanopowder to early life stages of the japanese medaka (*Oryzias Latipes*), *Chemosphere* 82 (7) (2011) 1002–1009, <https://doi.org/10.1016/j.chemosphere.2010.10.068>.
- [14] Q. Fang, X. Shi, L. Zhang, Q. Wang, X. Wang, Y. Guo, B. Zhou, Effect of titanium dioxide nanoparticles on the bioavailability, metabolism, and toxicity of pentachlorophenol in zebrafish larvae, *J. Hazard. Mater.* 283 (2015) 897–904, <https://doi.org/10.1016/j.jhazmat.2014.10.039>.
- [15] C. Botta, J. Labille, M. Auffan, D. Borschneck, H. Miche, M. Cabié, A. Masion, J. Rose, J.-Y. Bottero, TiO₂-based nanoparticles released in water from commercialized sunscreens in a life-cycle perspective: structures and quantities, *Environ. Pollut.* 159 (6) (2011) 1543–1550, <https://doi.org/10.1016/j.envpol.2011.03.003>.
- [16] M. Auffan, M. Pedetour, J. Rose, A. Masion, F. Ziarelli, D. Borschneck, C. Chanéac, C. Botta, P. Chaurand, J. Labille, J.-Y. Bottero, Structural Degradation at the Surface of a TiO₂-Based Nanomaterial Used in Cosmetics, *Environ. Sci. Technol.* 44 (7) (2010) 2689–2694, <https://doi.org/10.1021/es903757q>.
- [17] J. Labille, J. Feng, C. Botta, D. Borschneck, M. Sammut, M. Cabie, M. Auffan, J. Rose, J.-Y. Bottero, Aging of TiO₂ Nanocomposites Used in Sunscreen. Dispersion and Fate of the Degradation Products in Aqueous Environment, *Environ. Pollut.* 158 (12) (2010) 3482–3489, <https://doi.org/10.1016/j.envpol.2010.02.012>.
- [18] K.M. Tyner, A.M. Wokovich, D.E. Godar, W.H. Doub, N. Sadrieh, The state of nano-sized titanium dioxide (TiO₂) may affect sunscreen performance: nano-sized TiO₂ and sunscreen performance, *Int. J. Cosmet. Sci.* 33 (3) (2011) 234–244, <https://doi.org/10.1111/j.1468-2494.2010.00622.x>.
- [19] H. Kamiya, M. Iijima, Surface modification and characterization for dispersion stability of inorganic nanometer-scaled particles in liquid media, *Sci. Technol. Adv. Mater.* 11 (4) (2010) 044304, <https://doi.org/10.1088/1468-6996/11/4/044304>.
- [20] Y. Hanada, M. Nomura, H. Suzuki, H. Kamiya, Analysis of the dispersion behavior of surface-modified titanium dioxide nanoparticles in silicone oil using the colloid probe AFM method, *J. Soc. Powder Technol. Jpn.* 52 (3) (2015) 139–144, <https://doi.org/10.4164/sptj.52.139>.
- [21] M. Rossano, N. Hucher, C. Picard, D. Colletta, F. Le Foll, M. Grisel, Effects of aging on structure and stability of TiO₂ nanoparticle-containing oil-in-Water emulsions, *Int. J. Pharm.* 461 (1–2) (2014) 89–96, <https://doi.org/10.1016/j.ijpharm.2013.11.039>.
- [22] SaNogueira, J. P. (73) Assignee: Playtex Products, Inc., Westport, CT. 26.
- [23] D. Terescenco, N. Hucher, G. Savary, C. Picard, From interface towards organised network: questioning the role of the droplets arrangements in macroscopically stable O/W emulsions composed of a conventional non-ionic surfactant, TiO₂ particles, or their mixture, *Colloids Surf. Physicochem. Eng. Asp.* 578 (2019) 123630, <https://doi.org/10.1016/j.colsurfa.2019.123630>.
- [24] T. Imae, K. Muto, S. Ikeda, The PH dependence of dispersion of TiO₂ particles in aqueous surfactant solutions, *Colloid Polym. Sci.* 269 (1) (1991) 43–48, <https://doi.org/10.1007/BF00654658>.
- [25] F. Loosli, S. Stoll, Effect of surfactants, PH and water hardness on the surface properties and agglomeration behavior of engineered TiO₂ nanoparticles, *Environ. Sci. Nano* 4 (1) (2017) 203–211, <https://doi.org/10.1039/C6EN00339G>.
- [26] E. Núñez-Rojas, H. Domínguez, Computational studies on the behavior of sodium dodecyl sulfate (SDS) at TiO₂(Rutile)/Water interfaces, *J. Colloid Interface Sci.* 364 (2) (2011) 417–427, <https://doi.org/10.1016/j.jcis.2011.08.069>.
- [27] S. Skoglund, T.A. Lowe, J. Hedberg, E. Blomberg, I.O. Wallinder, S. Wold, M. Lundin, Effect of laundry surfactants on surface charge and colloidal stability of silver nanoparticles, *Langmuir* 29 (28) (2013) 8882–8891, <https://doi.org/10.1021/la4012873>.
- [28] Evonik. Tegosoft P - Technical Information, (2018).
- [29] SEPPIC. Easynov - Liquid Emulsifier, (2011) www.sepic.com.
- [30] Schlossman, M. L. PIGMENTS AND BASES INTO PRODUCTS CONTAINING OIL AND WATER PHASES. 6.
- [31] J. Chou, T.J. Robinson, H. Doan, Rapid comparison of UVB absorption effectiveness of various sunscreens by UV-vis spectroscopy, *J. Anal. Bioanal. Tech.* 08 (02) (2017), <https://doi.org/10.4172/2155-9872.1000350>.
- [32] L. Rowencyzyk, C. Duclairoir-Poc, M. Barreau, C. Picard, N. Hucher, N. Orange, M. Grisel, M. Feuillole, Impact of coated TiO₂-Nanoparticles used in sunscreens on two representative strains of the human microbiota: effect of the particle surface nature and aging, *Colloids Surf. B Biointerfaces* 158 (2017) 339–348, <https://doi.org/10.1016/j.colsurfb.2017.07.013>.
- [33] A. Vilgé-Ritter, A. Masion, T. Boulangé, D. Rybacki, J.-Y. Bottero, Removal of natural organic matter by coagulation-flocculation: a Pyrolysis-GC-MS study, *Environ. Sci. Technol.* 33 (17) (1999) 3027–3032, <https://doi.org/10.1021/es981232p>.
- [34] Y.-C. Chang, Y. Yamamoto, H. Matsumoto, Accumulation of aluminium in the cell wall pectin in cultured tobacco (*Nicotiana tabacum* L.) cells treated with a combination of aluminium and Iron, *Plant Cell Environ.* 22 (8) (1999) 1009–1017, <https://doi.org/10.1046/j.1365-3040.1999.00467.x>.
- [35] J.L. Yang, Y.Y. Li, Y.J. Zhang, S.S. Zhang, Y.R. Wu, P. Wu, S.J. Zheng, Cell wall polysaccharides are specifically involved in the exclusion of aluminum from the rice root apex, *Plant Physiol.* 146 (2) (2008) 602–611, <https://doi.org/10.1104/pp.107>.

- 111989.
- [36] K. Singh, S. Mohan, Adsorption Behavior of Selected Monosaccharides onto an Alumina Interface, *J. Colloid Interface Sci.* 270 (1) (2004) 21–28, <https://doi.org/10.1016/j.jcis.2003.05.002>.
- [37] K. Singh, S. Mohan, Kinetic studies of the sucrose adsorption onto an alumina interface, *Appl. Surf. Sci.* 221 (1–4) (2004) 308–318, [https://doi.org/10.1016/S0169-4332\(03\)00950-4](https://doi.org/10.1016/S0169-4332(03)00950-4).
- [38] G.H. Posner, Organic reactions at alumina surfaces, *Angew. Chem. Int. Ed. Engl.* 17 (7) (1978) 487–496, <https://doi.org/10.1002/anie.197804871>.
- [39] N.W. Gabel, C. Ponnampereuma, Model for origin of monosaccharides, *Nature* 216 (5114) (1967) 453–455, <https://doi.org/10.1038/216453a0>.
- [40] C. Reid, L.E. Orgel, Synthesis of sugars in potential prebiotic conditions, *Nature* (216) (1967) 455, <https://doi.org/10.1038/216453a0>.
- [41] A. Noel, D. Mirbel, E. Cloutet, G. Fleury, C. Schatz, C. Navarro, G. Hadziioannou, CyrilBrochon, Tridodecylamine, an efficient charge control agent in non-polar media for electrophoretic inks application, *Appl. Surf. Sci.* 428 (2018) 870–876, <https://doi.org/10.1016/j.apsusc.2017.09.171>.
- [42] S.K. Sainis, V. Germain, C.O. Mejean, E.R. Dufresne, Electrostatic interactions of colloidal particles in NoENMolar solvents: role of surface chemistry and charge control agents †, *Langmuir* 24 (4) (2008) 1160–1164, <https://doi.org/10.1021/la702432u>.
- [43] P.G. Smith, M.N. Patel, J. Kim, K.P. Johnston, T.E. Milner, Electrophoretic mobility measurement by differential-phase optical coherence tomography, *J. Phys. Chem. C* 111 (6) (2007) 2614–2622, <https://doi.org/10.1021/jp0645723>.
- [44] I.D. Morrison, Electrical charges in nonaqueous media, *Colloids Surf. Physicochem. Eng. Asp.* 71 (1) (1993) 1–37, [https://doi.org/10.1016/0927-7757\(93\)80026-B](https://doi.org/10.1016/0927-7757(93)80026-B).
- [45] K.D. Kwon, H. Green, P. Bjöörn, J.D. Kubicki, Model bacterial extracellular polysaccharide adsorption onto silica and alumina: quartz crystal microbalance with dissipation monitoring of dextran adsorption, *Environ. Sci. Technol.* 40 (24) (2006) 7739–7744, <https://doi.org/10.1021/es061715q>.